Local site effects in Ataköy, Istanbul, Turkey, due to a future large earthquake in the Marmara Sea

Mathilde B. Sørensen, Ivo Oprsal, Sylvette Bonnefoy-Claudet, Kuvvet Atakan, P.M. Mai, Nelson Pulido, Caglar Yalciner

Geophys. J. Int. (2007) **171,** 1363–1375 doi: 10.1111/j.1365-246X.2007.03598.x

A conjugate strike-slip fault system within the extensional tectonics of Western Turkey

Mustafa Aktar,[1] Hayrullah Karabulut,[1] Serdar Özalaybey[2] and Dean Childs[1]

[1] *Bogazici University, Kandilli Observatory and Earthquake Research Institute,* 81220 *Cengelkoy Istanbul, Turkey. E-mail: kara@boun.edu.tr*
[2] *TUBITAK-MRC, Earth and Marine Sciences Institute, Gebze, Kocaeli, Turkey*

Accepted 2007 September 1. Received 2007 September 1; in original form 2006 June 11

SUMMARY

Three main shocks M-1, M-2 and M-3 (17 October 2005 at 05:45 UTC, M_w 5.4; 17 October at 09:46 UTC, M_w 5.8 and 20 October at 21:40 UTC, M_w 5.9) and their associated aftershocks within the Gulf of Sığacık, 50 km southwest of Izmir, Turkey were studied in detail. A temporary seismic network deployed during the activity allowed the hypocentre of M-3 and subsequent aftershocks to be determined with high accuracy. A relative relocation technique was used to improve the epicentres of M-1 and M-2. All three main shocks have strike-slip mechanisms which agree with the linear trends of the aftershock locations. Two distinct zones were illuminated by the aftershock locations. The zones contain clear echelon patterns with slightly different orientations from the trend of the aftershock distribution. M-2 and M-3 ruptured along of the eastern rupture zone which aligns N45°E. However the strike direction of M-1 is not clearly identified. The alignment of the two rupture zones intersect at their southern terminus at an angle of 90°. The fault zones form conjugate pair system and static triggering is considered as a probable mechanism for the sequential west to east occurrence of M-1, M-2 and M-3. This earthquake sequence provides seismological evidence for conjugate strike-slip faulting co-existing within a region dominated by north–south extension and well-developed east–west trending normal faults.

Key words: Aegean Sea, aftershocks, conjugate faulting, extensional tectonics, focal mechanisms, western Anatolia.

INTRODUCTION

The Aegean Sea and Western Turkey are characterized by broad scale lithospheric extensional processes that result in crustal thinning and associated faulting (Angelier 1978; McKenzie 1978; LePichon & Angelier 1981; Şengör *et al*. 1984). Several large-scale graben structures oriented E–W dominate the region (Bozkurt 2001). Large destructive earthquakes have occurred within these grabens, nearly all of them having normal mechanisms striking E–W that fit well with N–S extensional tectonics (Eyidoğan & Jackson 1985). However in the last 20 yr several moderate size earthquakes ($M > 5.0$) with strike-slip mechanisms were recorded (Fig. 1). Most of these events have strikes which orient obliquely to the E–W trending structures and they are mostly located in zones that lay between the grabens. Recent studies based upon surface morphology (Emre & Barka 2000) and using marine seismic reflection data (Ocakoğlu *et al*. 2004; Ocakoğlu *et al*. 2005) provide evidence of active strike-slip faults in the area. Analogue models that were developed to simulate the extensional processes of the Aegean (Gautier *et al*. 1999) also demonstrate that oblique strike-slip features can be generated. Accurate description of the seismic activity and details of active faults are crucial in order to understand the nature of the strike-slip fault systems existing between the large graben structures.

In this paper, we studied an earthquake sequence that occurred from 2005 October 17 to 20 within the Gulf of Sığacık, south of the Karaburun Peninsula (Fig. 1) near Izmir, Turkey. Three main shocks occurred within a time window of 3 d. The improved state of permanent seismic networks in the region together with an additional installation of a temporary network allowed unprecedented accuracy in the determination of hypocentre locations and the rupture geometry for this sequence. The seismic sequence started with two main shocks (M-1 and M-2, respectively) separated by 4 hr (2005 October 17 at 05:45 UTC, $M_w = 5.4$; October 17 at 09:46 UTC, $M_w = 5.8$). Following the occurrence of M-1 and M-2, four temporary stations were installed within 10 km of the epicentres in order to monitor the aftershock activity closely. Immediately after the installation of the temporary network a third main shock (M-3) occurred (October 20 at 21:40 UTC, $M_w = 5.9$). Data from the temporary network allowed the hypocentre of the third main shock to be determined with good accuracy. Relative relocation techniques were subsequently used in order to locate M-1 and M-2. The relocations combined with high quality aftershock locations indicate two

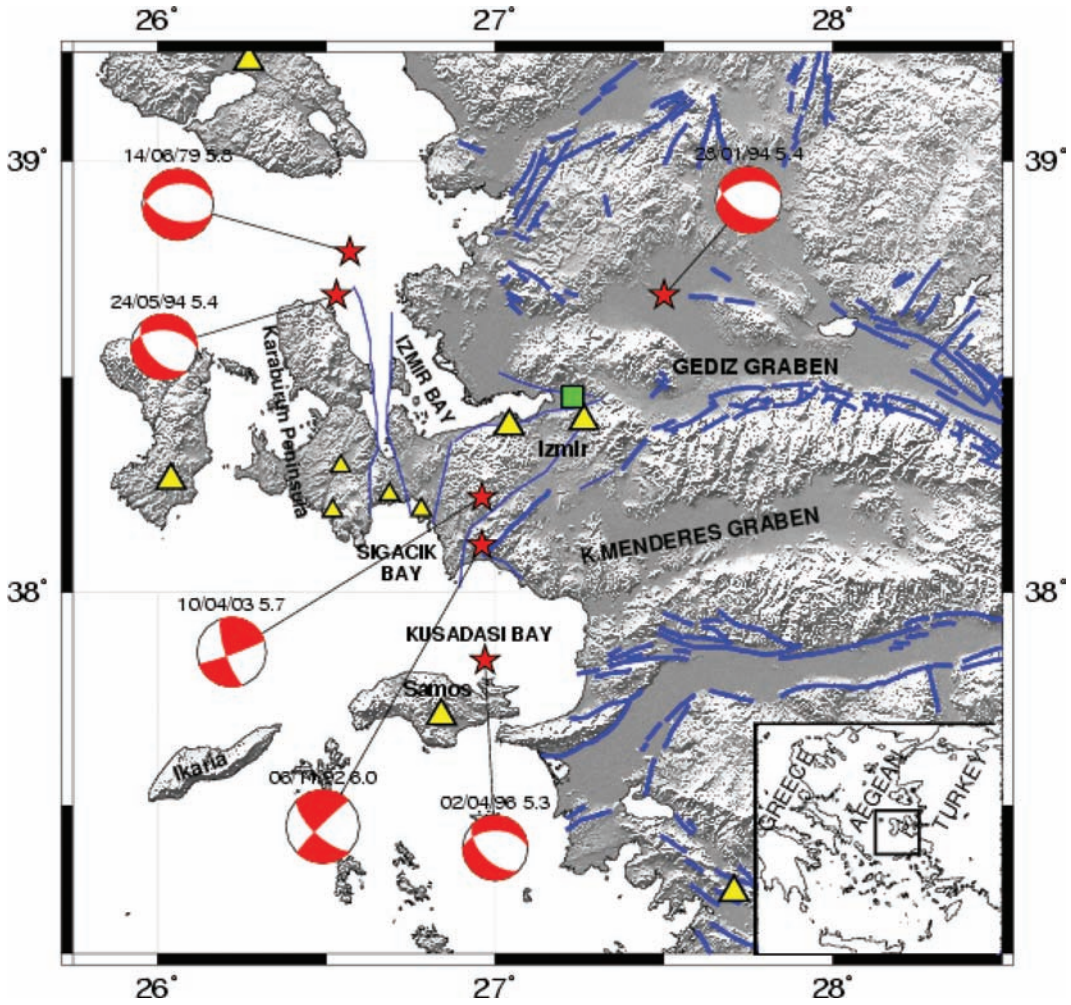

Figure 1. A general view of seismogenic features around the Sığacık Bay. Thick black lines indicate active normal faults (after Şaroğlu *et al*. 1992). Thin black lines around Sığacık Bay show the compilation of faults based on recent studies (Genç *et al*., 2001; Ocakoğlu *et al*. 2004; Emre *et al*. 2005). Focal mechanisms and locations of the earthquakes that have occurred within the last 30 yr with magnitude greater than 5.5 are also shown (USGS, NEIC). Large triangles show the permanent seismic stations in the region, the small triangles shows temporary stations and square shows the location of the acceleration station (URL).

distinct zones nearly orthogonally oriented forming a conjugate fault system.

TECTONIC SETTING

It is widely accepted that the southern Aegean Sea and Western Turkey are currently undergoing a continental lithospheric extension in the N–S direction (McKenzie 1972; Angelier 1978; McKenzie 1978; LePichon & Angelier 1981; Şengör *et al*. 1984). However the arguments diverge when it comes to explain the driving mechanism of this extension process. Some authors associate the extension with slab pull of the retreating Hellenic Subduction Zone (McKenzie 1978; LePichon & Angelier 1979). Other authors (McKenzie 1978; Dewey & Şengör 1979, Taymaz *et al*. 1991) assert the westward extrusion of the Anatolia due to Arabia–Eurasia collision as the major agent for the extension. In recent years extensive GPS surveys have shown that a single unified plate motion cannot account for the observed crustal movements and deformations. The modern paradigm that deformation pattern of continental lithosphere is far more complex than the oceanic one applies well to the Aegean. There is convincing evidence that the region is formed by an assembly of microplates of which the exact number and boundaries is an area of active research. (Nyst & Thatcher 2004). In this context accurate location of earthquakes together with well-identified active fault systems provide a keyrole in identifying the boundaries of the assumed microplates.

As a primary characteristics of the most extensional provinces worldwide, well-developed E–W trending grabens, located both inland and off-shore are the dominant structural feature of Western Turkey (Angelier *et al*. 1981; Yılmaz 1997; Kurt *et al*. 1999; Yılmaz *et al*. 2000; Genç *et al*. 2001). Well studied and instrumentally recorded earthquakes with magnitudes up to 7.0 located along normal faults bounding the graben features constitute the first order seismological evidence for the extensional tectonics within this region (Eyidoğan & Jackson 1985; Taymaz *et al*. 1991; Kiratzi & Louvari 2003). More recently, deformation inferred from extensive GPS surveys shows N–S oriented crustal extension which increases in amplitude from north to south (Kahle *et al*. 1998; Hurst *et al*. 2000; McClusky *et al*. 2000). The northern Aegean is dominated mostly by strike-slip faults and in particular the North Anatolian Fault along the Marmara Sea and possibly most of the North Aegean

trough (Taymaz *et al*. 1991; Karabulut *et al*. 2006). A component of extensional nature is also observed in the north but as a secondary constituent to the dominant dextral shearing. The issue of the co-existence and interactions between strike-slip and normal faults systems is presently a topic of active debate particularly for the case of the Marmara Sea in the context of seismic hazard related to the city of Istanbul (LePichon *et al*. 2001; Armijo *et al*. 2002). Although the interactions of two types of faulting are much discussed for the northern Aegean and Marmara regions, no major arguments have been proposed for similar features observed in the southwest of Turkey. Recently, Ocakoğlu *et al*. (2005) reported evidence from marine seismics for extensive strike-slip faulting in the vicinity of the Karaburun Peninsula. Their explanation for the presence of this observed strike-slip faulting was based on the hypothesis of E–W compression in addition to the well-documented N–S extension. A local GPS survey in the surroundings of Izmir revealed a differential motion between Karaburun Peninsula and the mainland in addition to the extension (Aktuğ & Kılıçoğlu 2006).

Large destructive earthquakes are documented for the 19th century (Altınok *et al*. 2005) however this type of information lacks accuracy and reliability necessary to understand their relation with the active faults. Earthquakes of magnitude greater than 5.5 have been instrumentally recorded during the last 50 yr, however none of them have correlated well with surface fault mapping (Fig. 1). Large uncertainities in epicentre locations on the order of 20 km due to poor station coverage may be the primary reason for the lack of correlation. Fault plane solutions for these events were obtained from teleseismic data (Kiratzi & Louvari 2003) and the strike directions show predominant NE–SW or NW–SE orientation. Fault mapping based on surface observations and areal photography analysis in the Karaburun Peninsula dominantly gave N–S strike direction (Genç *et al*. 2001; Emre *et al*. 2005; Ocakoğlu *et al*. 2005).

DATA ANALYSIS

The seismicity in the vicinity of the Karaburun Penisula is continuously monitored using permanent stations located both on the Turkish mainland and on the Dodecaneese Islands of Greece. Since the average spacing of permanent stations is on the order of 100 km location accuracy is not sufficient to illuminate structures on a local scale. A four station temporary network, consisting of three-component Mark Products L-28 short period sensors recorded by Reftek 130 24-bit digitizers, was deployed on 19 October, 2005, 36 hr after the occurrence of the first main shock (M-1) and 6 hr before the occurrence of M-3. The data were recorded continuously for 1 month. More than 3500 events were located during the first 7 d of the installed local network and 3200 of them with the best accuracy were selected for the present analysis. The majority of the located aftershocks occurred after M-3 (Fig. 2a). We also used the continuous seismic data and available readings from stations operating in the region (Fig. 1). A 1-D crustal velocity model was obtained using the VELEST inversion code (Kissling *et al*. 1994). Initial locations were obtained using hypoinverse location code (Klein 1989). Both *P* and *S* arrivals from temporary stations were used in determining the locations and the average rms error of the traveltimes for the 3200 events was less than 0.05 s.

The location of hypocentres were well constrained by the closely located temporary stations and the addition of readings from the nearby permanent stations reduced the error ellipsoid down to 0.9 km in longitude, 1.4 km in latitude and 2 km in depth (Figs 2c–e). Since the error ellipsoid only depends on the accuracy of the phase picks and the geometry of the stations, the true uncertainty which depends on many other factors including the velocity model should be higher. We relocated aftershocks using both the Double-Difference (Waldhauser & Elseworth 2000) and the Source-Specific Station Term (SSST) methods (Lin & Shearer 2005). Both methods lead to a limited improvement in the locations probably due to the use of relatively low number of stations. Fig. 3 illustrate the results obtained using the SSST method.

Local magnitudes were calculated and show a lower threshold of 1.0. The magnitude of largest aftershock recorded by the temporary network was 4.6. The catalogue is complete down to the magnitude of 1.7. Slightly different *b*-values were obtained for two branches giving 0.9 for the western and 0.8 for the eastern one.

MAIN SHOCK LOCATIONS AND SOURCE MECHANISMS

The epicentre of M-3 was well constrained using the high quality data from the temporary network. However, the locations of M-1, M-2 and their aftershocks which occurred before the installation of temporary network had uncertainties on the order 10 km due to poor station coverage and did not provide any definitive insight on the geometry of the rupture zones. To improve the epicentre locations of M-1 and M-2 we used a relative location technique. Using M-3 as the master event, M-1 and M-2 were relocated using *P*-wave arrival time differences to all stations within a 1500 km radius of the epicentre. Assuming that the depth of the three events are similar, the relative *P* arrival time differences between events should follow a sine curve if plotted against the azimuth of the stations relative to the epicentre. The similar depth assumption is not critical since any difference in depth between two events will mainly shift the sine curve up or down but not significantly modify its shape. If such a sine curve can be estimated, the relative distance between the two events is obtained from the amplitude and the azimuth of the second event with respect to the master event can be taken from the phase angle of the sine curve. The results of this analysis are shown in Figs 3A and B. All three main shocks are located off-shore within the Gulf of Sığacık and activated consecutively from west to east. The depth of the M-3 is well resolved by the use of high quality temporary network data. The depth of the first and second events however were re-estimated only using the permanent network data by fixing the horizontal locations obtained from the relative location analysis.

Fault plane solutions of the main shocks and some of the large aftershocks obtained by several agencies (USGS, Harvard, ETH) using teleseismic and regional wave inversion techniques were in agreement with each other. We also used the first motion polarity approach in order to improve the sensitivity of the strike direction. All three main shocks gave strike-slip mechanisms with M-2 and M-3 having nearly the same strike. Focal mechanisms of some of the large aftershocks recorded during the deployment of the temporary network are also determined. The strike errors of the focal mechanisms is less than 2º for the three main shocks and less than 5° for the aftershocks. The results are summarized on Table 1 and the fault plane solutions (FPS) of the main shocks and three aftershocks are presented in Appendix Fig. A1.

ANALYSIS OF THE ACTIVITY

The aftershock activity is clustered in two distinct zones which are roughly perpendicular to each other (Fig. 4). Events recorded during

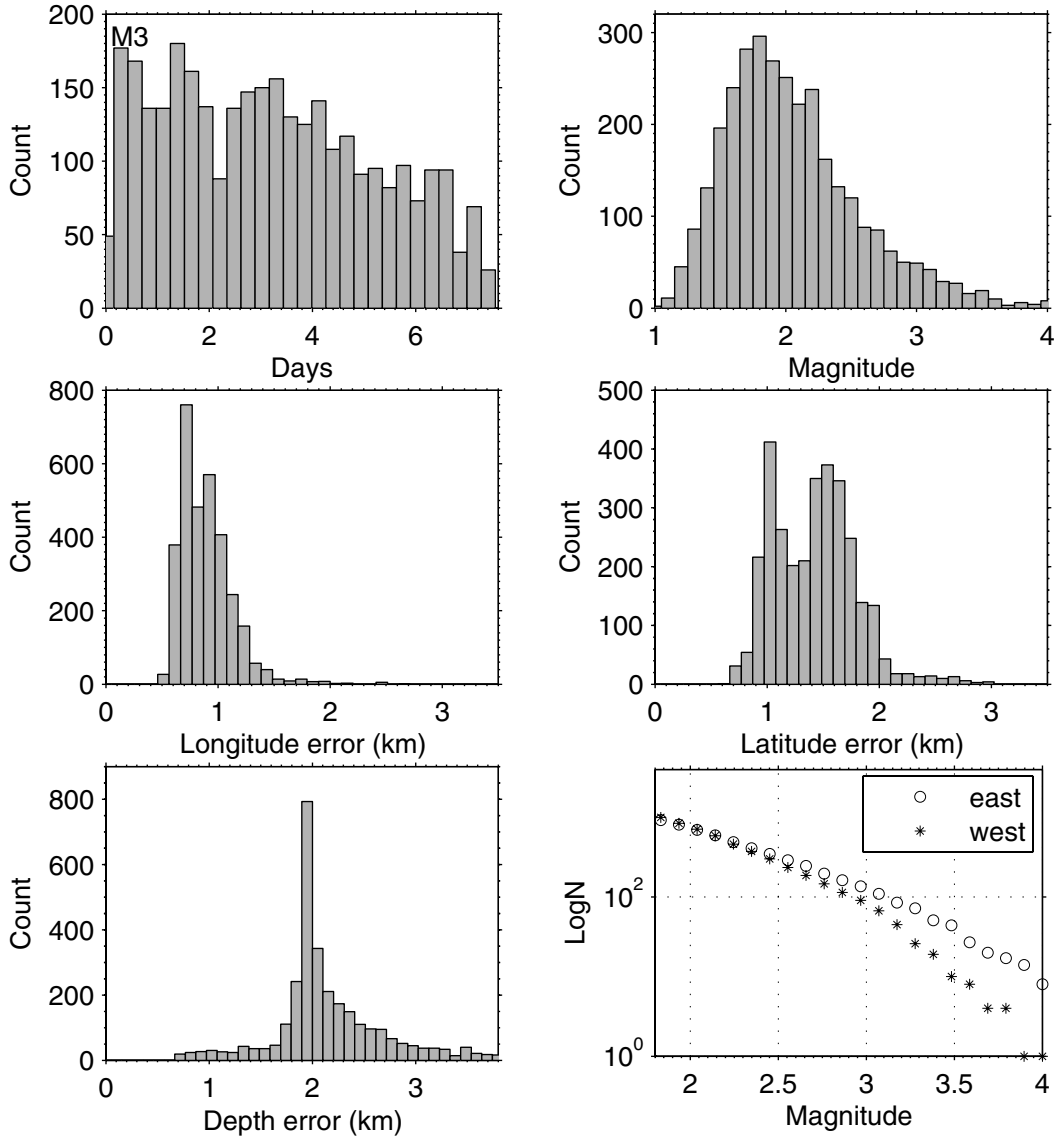

Figure 2. Statistics of the located aftershocks: (a) occurrence of aftershocks during the 7 d of the operated network; (b) magnitude distribution; (c) latitude errors; (d) longitude errors; (e) depth errors and (f) frequency magnitude relations of two branches.

the first 6 hr after the installation of the temporary network largely correspond to the aftershock activity of M-1 and M-2 . The epicentre of M-1 is located on the southern terminus of the western rupture zone which lies off the western coast of the Sığacık Bay. The activity partly extends on land with a strike of N25°W. The location of the M-1 does not let us to associate the event with a particular branch with confidence. The fault planes obtained by focal mechanism solutions are consistent with the orientation of both zones.

M-2 which occurred 4 hr after M-1 was located in the eastern aftershock zone which aligns along a strike of N48°E. M-3 is located on the northeastern terminus of the eastern zone extending the rupture zone of the M-2 further to the NE (Fig. 3). Majority of the aftershocks located in this study occurred after M-3 (October 20 21:30, $M_w = 5.9$) and are concentrated within the eastern zone. Fig. 5 shows 3-D view of the activity zone and two depth sections oriented along the long axis of both the western and eastern branches. The depth of the aftershock activity is confined to a seismogenic zone between 5–11 and 8–13 km for the western and eastern branches, respectively. The aftershock activity is concentrated at shallower depths than the nucleation points of the three main shocks. This indicates that the rupture started at the bottom of seismogenic zone and propagated upwards to shallower depths as it has been observed in similar strike-slip earthquakes in the region (Özalaybey *et al*. 2002).

The two branches observed from the seismicity do not define simple planar fault zones. We clearly observe in the western branch that fault segments form an echelon array with individual segments at slightly different orientation from the general trend of the fault zone. However such segmentation is not obvious within the eastern branch. This is partly due to the larger latitude errors resulting from the orientation of the seismicity with respect to the station geometry (Fig. 2d). Considering the size of M-2 and M-3 the length of the ruptured zone is expected to reach 10 km in total. However the observed aftershock zone only covers approximately 6 km. The 3-D view and the depth sections shows localizations of aftershocks which align at slightly different orientation from the strike direction of M-2 and M-3. This is an indication that the activity is distributed over an array of weakness zones. An aftershock of magnitude 4.6

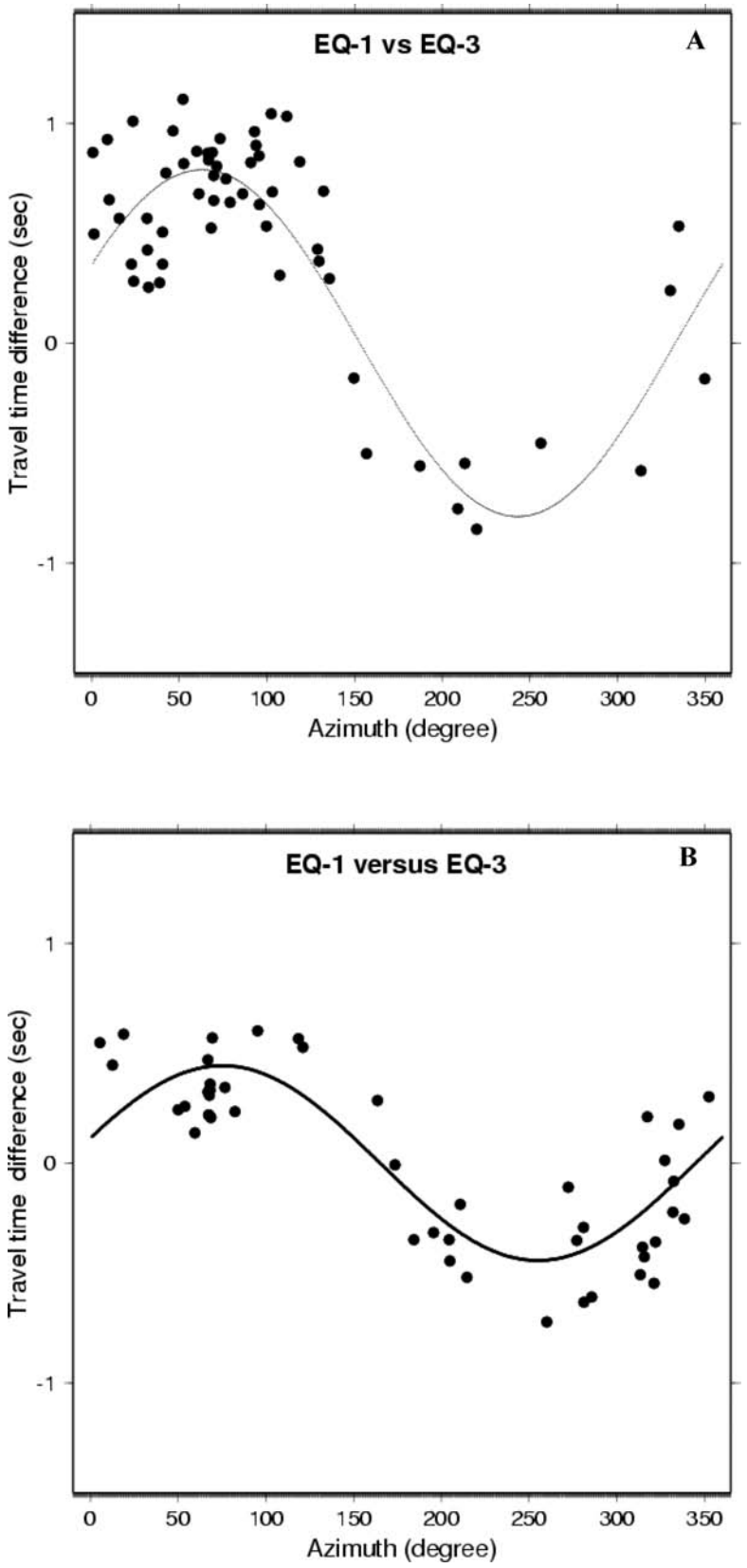

Figure 3. Relative relocation of M-1, (17 October, 2005 05:45 UTC, M_w 5.4) and M-2 (17 October, 2005 09:46 UTC, M_w 5.8) referenced to M-3 (20 October, 2005 21:40 UTC, M_w 5.9) which was located from the temporary network data. The azimuthal variation of the differential P-phase arrival times at each station (shown as black dots) for events M-1 and M-2 relative to M-3 recorded at regional stations are shown in A and B, respectively. Sine curve fitted in the least-squares sense is also shown in the figure. Since the majority of the seismic stations are located within epicentral distances between 200–1000 km, the first *P*-arrival is Pn which travels roughly at a velocity of 8.0 km s^{-1}. The azimuth of the relocated event with respect to the reference event is given by a phase shifted sine curve. Only *P*-phase picks with timing accuracy of 0.1 s were used in the analysis, therefore, plots (A) and (B) have different station suites.

Table 1. Focal parameters of three main shocks and three aftershocks.

	Origin time	M_w	Lat	Lon	Depth	Strike	Dip	Rake
M-1	17/10/2005 05:45	5.4	38.166	26.637	11	246	82	−172
M-2	17/10/2005 09:46	5.8	38.174	26.676	11	238	85	177
M-3	17/10/2005 21:40	5.9	38.191	26.696	10	50	84	−172
A-1	22/10/2005 01:05	3.6	38.223	26.612	8	320	76	7
A-2	22/10/2005 15:34	3.6	38.183	26.630	9	334	80	−9
A-3	22/10/2005 11:47	4.6	38.159	26.612	9	150	90	0.0

with a similar mechanism to the M-1 located SW of the junction also provide evidence for the presence of such weakness zones (Fig. 4B).

STRONG MOTION MODELLING

The only accelerograph station at the proximity of the activity zone was located on the northeast at distances of 60, 58 and 57 km away from the three main shocks, respectively (Fig. 1). The station is located on a hard rock site and maximum accelerations recorded at the station were 17, 22 and 36 mg for three main shocks, respectively. The azimuth of the station is approximately same as the fault planes of M-2 and M-3 and the orientation of the eastern branch of activity. Therefore, we expect that the ground motion appears mostly on the transverse component of the recordings (Bouchon 1981). The displacements for three main shocks are obtained by integrating the accelerograph records twice and only the transverse components are displayed on Fig. 6.

We modelled the transverse component of the displacement in order to verify the parameters such as focal mechanisms and depths of the three main shocks and to possibly infer the rupture directions. The velocity model for the modelling is given in Table 2. The earthquakes are modelled as propagating faults imbedded in a layered media (Bouchon 1982; Bouchon *et al*. 2000). The rupture starts at one of the lower corners (hypocentres) of the rectangular fault plane and spreads radially. The computation is carried out by representing the source as a superposition of shear dislocations points distributed over the fault plane. The ground displacements were calculated using discrete wavenumber method (Bouchon 1981).

The previously determined focal mechanisms were tested for various hypocentral depths between 9 and 13 km to search for a best-fitting model. The fault parameters leading to the best results are given in Table 3 and the waveform fits are shown on Fig. 6. Initial tests have shown that the simulation results were not sensitive to the variations of the rupture velocity held within realistic limits (2.0–3.0 km s^{-1}), we therefore, fixed it at 2.5 km s^{-1}. The sensitivity for the rupture directions was tested for the three earthquakes. The two extreme cases in which the rupture starts at the epicentre and propagates unilaterally away from the station and towards the station are illustrated in Fig. 6. The epicentral distances were same for both rupture directions. The synthetic waveforms were most sensitive to the thickness and shear wave velocity of the uppermost layer and the focal depths. The large kinks are the results of the reflections in the uppermost layer and are not related to any source complexity. These reflection can only be observed when peaks are sufficiently narrow so that they can be distinguished from each other. This is only happens when the rupture propagates towards the station due to the directivity effects.

The best fits for earthquakes M-2 and M-3 were obtained when the rupture is assumed to propagate towards the station, that is, in NE direction. For the smaller event M-1 located near the junction of two conjugate system, the tests were not conclusive to resolve neither the nodal plane nor the directivity (Fig. 6B). This is mainly due the smaller size of M-1 and larger distance to the station, which limits the resolution of the strong motion analysis. .

DISCUSSIONS AND CONCLUSIONS

The main shocks (M-1, M-2 and M-3) and the aftershocks reveal what appears to be a conjugate fault system which consists of two fault zones with strike-slip character intersecting with a north facing interior angle of 90°. The directivity analysis of the main shocks M-2 and M-3, together with the NE–SW trending aftershock pattern on the eastern branch leaves no doubt about the right lateral character of these two main shocks. On the other hand, the unresolved directivity for the main shock M-1 makes either of the nodal planes equally likely to be the true fault plane. However, we note that the main shock M-1 is located on the western branch which is clearly isolated from the eastern one by a gap of 3–4 km. Furthermore, a number of large aftershocks located along the western branch all gave nearly identical FPS which fits well the general alignment of the aftershocks, strongly supporting that the western branch essentially reflects left lateral character in the NW–SE direction. Therefore, despite the lack of direct evidence, we believe that M-1 located on the western branch is very likely to have the same mechanism which is left lateral in N25°W direction. Regardless of the arguments on the fault plane for the M-1, the clear V-shape pattern formed by the intersection of the two aftershock lineaments indicates the existence of a conjugate fault system in Sığacık Bay. A close look at the seismicity pattern, particularly at the western branch show clear evidence that the fault zone is not constrained to a single fracture line but to a complicated pattern of smaller segments of 4–5 km each and subparallel to each other. These type of a particular segmentation is called vein arrays and are known to exist in conjugate fault systems (Kelly *et al*. 1998).

Conjugate strike-slip fault systems may fit well within the N–S oriented extensional regime of western Turkey. Gautier *et al*. (1999) have modelled viscous flow under gravitational force to simulate the Aegean extension. Their analogue models have shown that extensional processes generate large numbers of intersecting strike-slip curvilinear faults with north facing concavity and at a later stage of the extensional history large grabens start to dominate the general morphology. Ganas *et al*. (2005), in their study of the 2001 Skyros earthquake ($M_w = 6.4$), mention other examples of strike-slip faults in the central Aegean that form conjugate fault systems. The 2005 October Gulf of Sığacık earthquake sequence provides strong seismological evidence for an active conjugate fault system within the region.

It is not uncommon to observe intersecting faults slipping during the same sequence. Both the Gamura and Yamada faults ruptured nearly simultaneously during the 1927 Tango earthquake on two orthogonal planes (Yeats *et al*. 1997). The Superstition Hills and Elmore Ranch earthquakes of 1987 November 23 and 24 are other

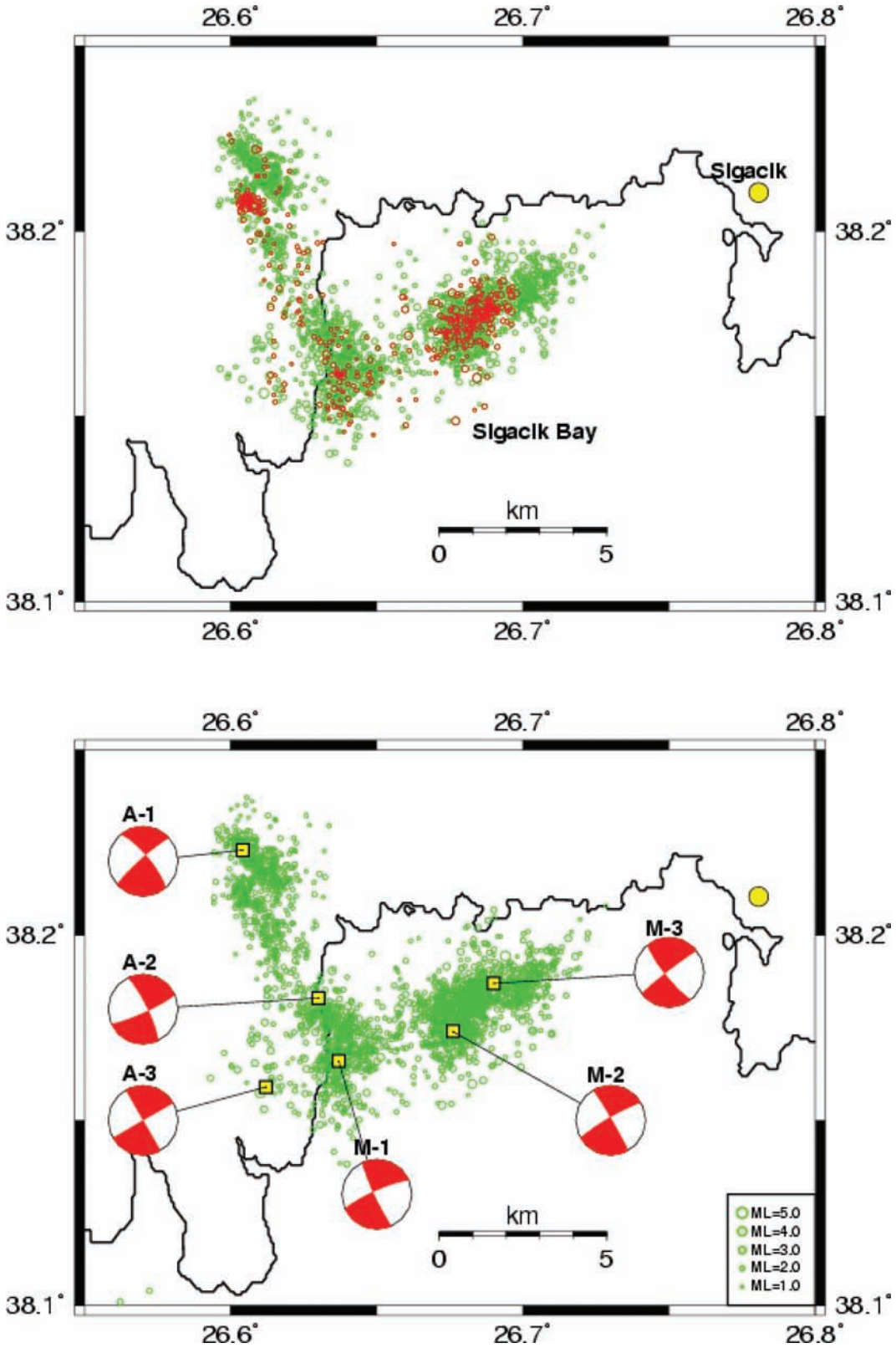

Figure 4. The aftershocks which occurred between the dates of 17 July 2005 and 25 July 2005 and located using Hypoinverse (Klein 1989) (above) and SSST (Lin & Shearer 2005) methods (below). The red circles on the above figure shows the aftershocks following M-3. The squares are the locations of the three main shocks.

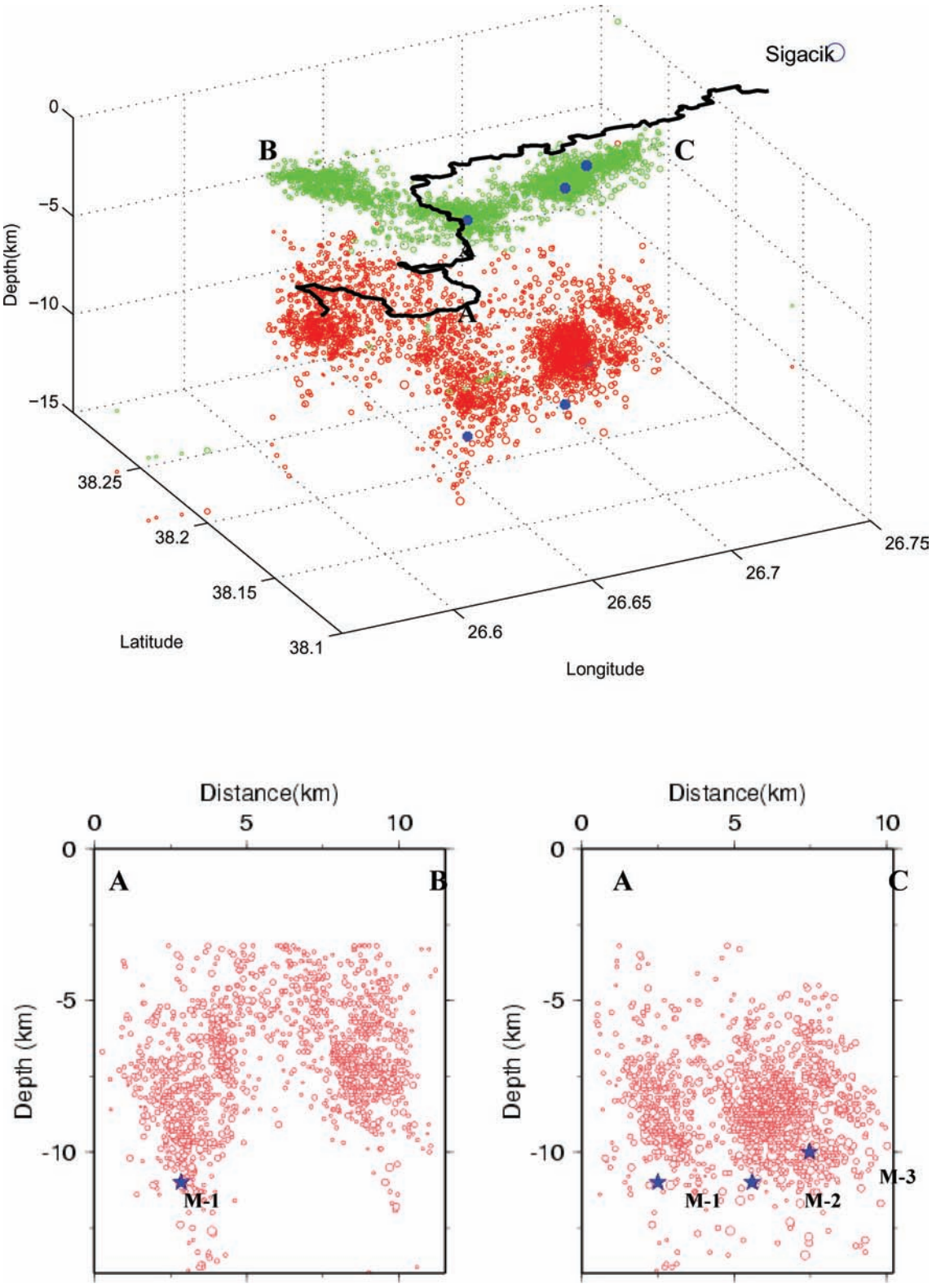

Figure 5. 3-D view of aftershocks (above) and depth view of the profiles along the AB and AC (below).

examples of intersecting faults (Yeats *et al*. 1997). The fault systems triggered by mutual static stress transfer mechanism have been studied in detail (Hudnut *et al*. 1989; Thatcher & Hill 1991). This stress transfer mechanism (Stein *et al*. 1992) may provide an explanation for the interaction of three main shocks that occurred within a relatively short time (4 and 50 hr) and distance (5 and 3 km). Benetatos *et al*. (2006) provides a triggering mechanism based on Coulomb criteria although the locations of the nucleation points of the three main shock are slightly different than the locations presented in this study.

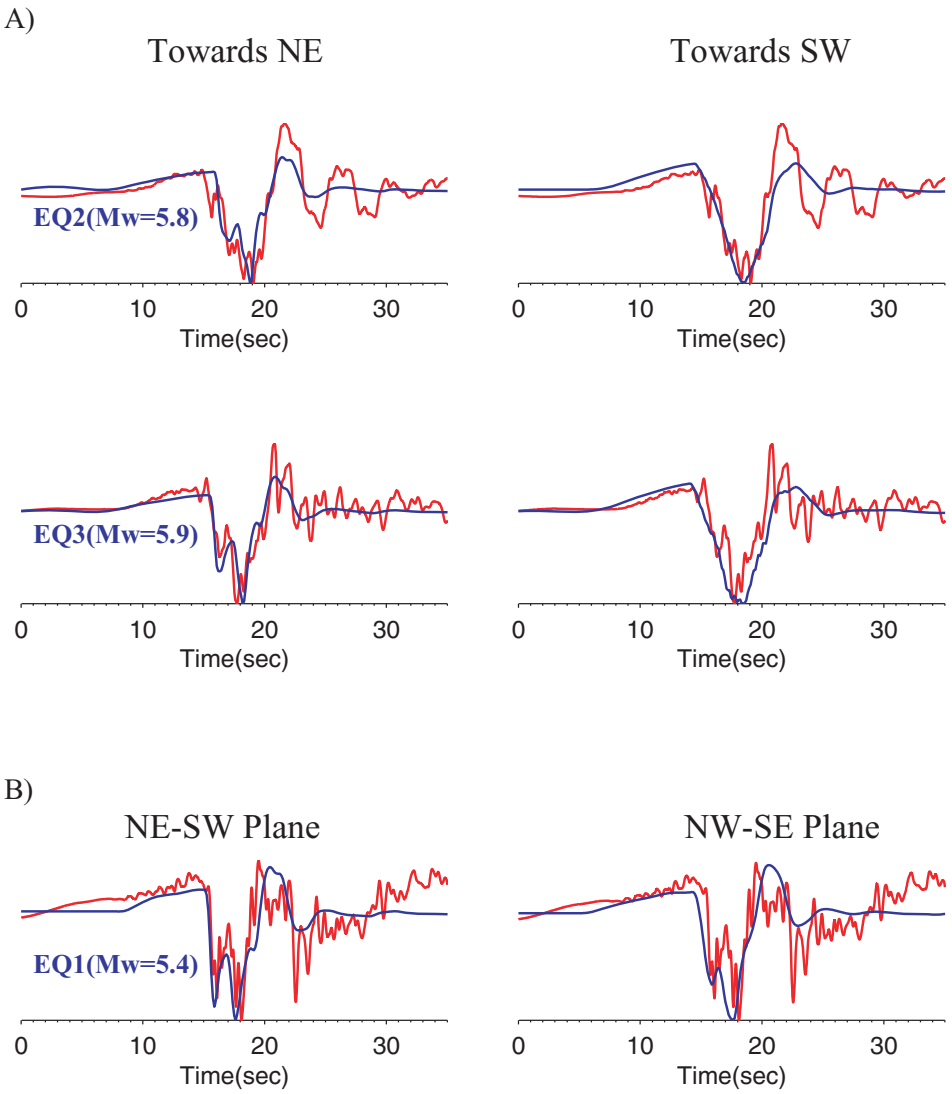

Figure 6. Strong motion modelling of the transverse component of the three earthquakes recorded at URL station (Observed = red, calculated = blue). (A) Left : rupture propagates towards the station and right: rupture propagates away from the station, (B) Left : rupture propagates towards the station on the NE plane and right: rupture on the NW plane for M-1.

Table 2. Velocity model.

Depth (km)	*Vp* (km s^{-1})	*Vs* (km s^{-1})
3.00	4.0	2.20
18.0	5.3	2.95
30.0	6.0	3.40
	7.9	4.50

In recent years much effort is devoted to identify and verify the microplates that are assumed to constitute the Aegean region. In general GPS data provides the general kinematics of such microplates while accurate earthquake locations may reveal the boundaries. Nyst & Thatcher (2004) have recently made a summary of various proposed models. In this context intersecting active fault structures supported by well-located earthquakes such as conjugate fault systems may provide clues to explain the complex interaction and the geometry of microplates. Recent GPS observations favour the assumption that the study area lies at the boundary of at least two different microplates: the Central Anatolia and the Southern Aegean (McKenzie 1978; Taymaz *et al*. 1991; McClusky *et al*. 2000; Nyst & Thatcher 2004). Models show slight variations over the exact block boundaries and behaviour. Aktuğ & Kılıçoğlu (2006) recently carried out a local GPS survey and used the velocity field to obtain the strain rates. They indicated a westward increasing extension in Izmir Bay and a clockwise rotation of the Karaburun Peninsula. They also postulated the existence of a small size block, squeezed between the Karaburun Peninsula and the mainland, which they called the Urla Block. The present study is consistent with the existence of this block of which the boundaries probably coincide with two branches of the conjugate fault system.

We present the velocity field obtained by Aktuğ & Kılıçoğlu (2006) with respect to a different reference velocity vector in order to emphasize the relative motion between Karaburun Peninsula and the mainland (Fig. 7). The change on the direction of velocity vectors across Izmir Bay shows a significant relative motion between the Karaburun Peninsula and the mainland indicating a transition zone roughly oriented in NS direction. The plate boundary between South

Table 3. Rupture parameters of the three main shocks

Main shocks	M_w	Length (km)	Vr (km s^{-1})	Slip (m)	Correlation (SW)	Correlation (NE)
M-1	5.4	4	2.5	0.8	0.67	0.63
M-2	5.8	5	2.5	1.0	0.85	0.83
M-3	5.9	5.5	2.5	1.0	0.83	0.83

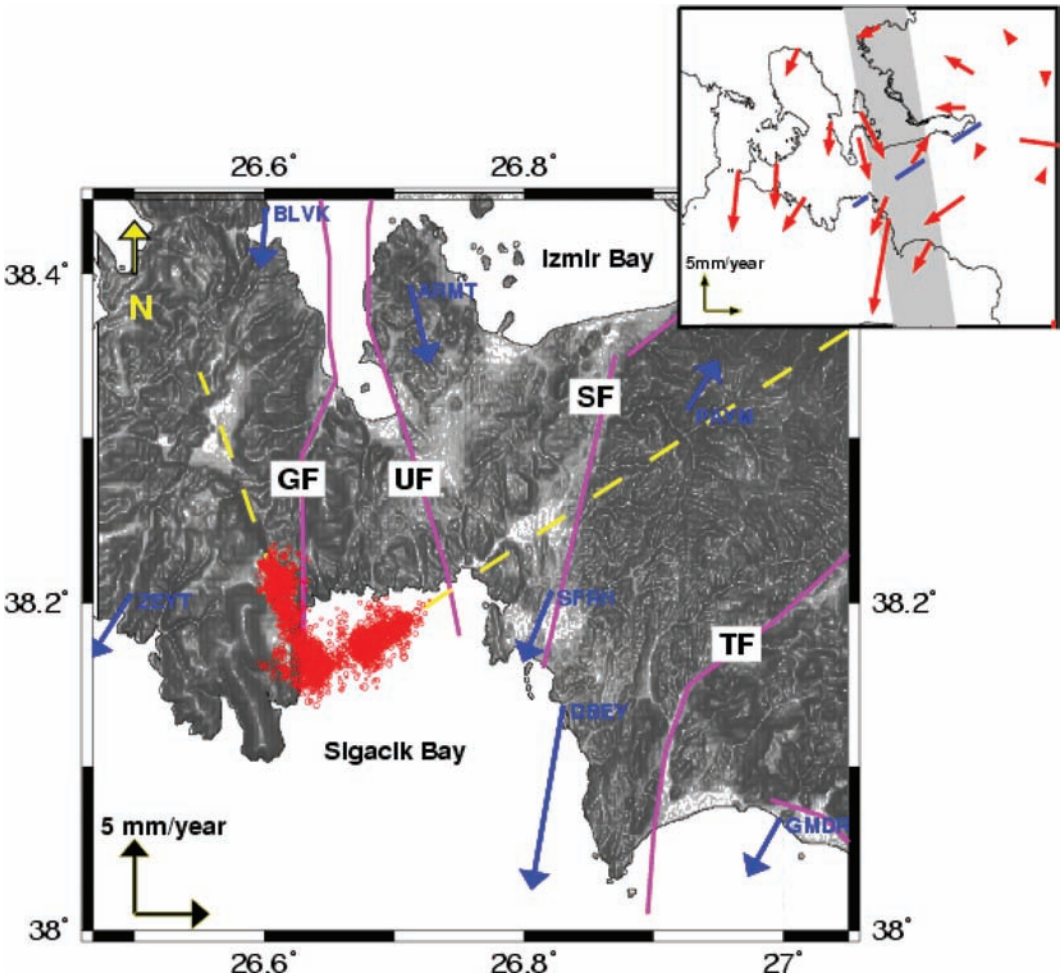

Figure 7. Illustration of the observed seismicity together with the GPS vectors and active faults in the region. Horizontal velocities shown in IPRF2000 frame are taken from Aktuğ & Kılıçoğlu (2006). The active faults (GF, Gülbahçe Fault; UF, Urla Fault; SF, Sıgacık Fault; TF, Tuzla Fault) are from Ocakoğlu *et al*. (2004); Emre *et al*. (2005); Genç *et al*. (2001). The top map shows velocity vectors at regional scale, indicating different trends on both side of the inferred microplate boundary (Nyst & Thatcher 2004), which is shown in grey band. The bottom figure shows the inland extension of the conjugate fault system (dashed lines). The velocity vectors are plotted with respect to a the reference velocity defined by $V_{east} = 1.5$ mm yr^{-1} and $V_{north} = -3.5$ mm yr^{-1}.

Aegean and Anatolia that was proposed by Nyst & Thatcher (2004) roughly corresponds to the same transition zone. The western branch of the conjugate fault system together with other NS oriented fault system in the area (Gülbahçe Fault, Urla Fault) may be considered as part of this transition zone. Different authors identified active faults in the Karaburun Peninsula based mainly on surface morphology. A compilation of the major fault lines are depicted in Fig. 5. The ones that are located close to the seismic activity are the Gülbahçe Fault (Emre *et al*. 2005), also named as the Karaburun Fault (Ocakoğlu *et al*. 2005) and the Urla Fault (Ocakoğlu *et al*. 2004, 2005). We note that M-1 occurred close to the Gülbahçe Fault. This is a N–S trending fault located off-shore for the most part and follows the western coastline of the Sığacık Bay. However, the strike direction of M-1 given by its fault plane solution as well as the trend of the aftershock activity are significantly different than the Gülbahçe Fault (Fig. 5). It is therefore, unlikely that M-1 corresponds to the activation of the Gülbahçe Fault.

The origin of the eastern branch however is connected to a different structure than the western one and is probably related to the westerward extension of the Gediz Graben. It constitute another example of NE–SW oriented right lateral strike-slip faults that splays from Gediz Graben, such the Tuzla fault and the Seferhisar Fault. These faults are likely to continue into the Aegean Sea (Goldsworthy *et al*. 2002) where they possibly connect to other major strike-slip structures such as the North Ikarian Basin (Lykousis *et al*. 1995). There is mapped fault that can be directly associated with the M-2 and M-3. We use the GPS data to constrain the inland prolongation of the eastern branch towards NE. If the eastern branch is extended NE, we note that the two stations (SFRH and PAYM) are located on both side of this prolongation line which can be considered as

hypothetical fault line. Their relative motion, if projected along the direction of the hypothetical fault (i.e. N44°E) shows an annual displacement of 7 mm yr^{-1}. This not only implies that the eastern branch of the conjugate fault continues inland in the NE direction but may also provide a rough estimate on the location and the annual slip rate. These type of NE–SW oriented strike-slip faults, (also including Tuzla Fault and Seferhisar Fault) are considered as subparallel transfer fault systems that terminate, splay or occasionally connect major graben structures. The latter takes up most the extensional movement, we therefore, do not expect that these strike-slip faults are able to produce large earthquakes comparable those found along major plate boundaries, such the North Anatolian Fault. Assuming that the maximum length of these faults is bounded by the average separation distance between grabens, the magnitude of the largest earthquake that may occur in the area is limited to about 6.5 (based on a maximum rupture length of 40 km). However, being closely located to densely populated settlements they still constitute a serious hazard for cities such as Izmir.

ACKNOWLEDGMENTS

We are thankful to TUBİTAK-Marmara Research Center for providing the instruments. We also would like to thank Michel Bouchon for discussions on strong motion modelling and Esen Arpat on the tectonics of the region. The paper benefited from comments by Thomas Plenefisch and Marco Bohnhoff. Partial support was provided by Boğaziçi University research fund under contract 03R103.

REFERENCES

Aktuğ, B. & Kılıçoğlu, A., 2006. Recent crustal deformation of Izmir, Western Anatolia and surrounding regions as deduced from repeated GPS measurements and strain field, *J. Geodyn.,* **41,** 471–484.

Altınok, Y., Alpar, B., Özer, N. & Gazioğlu, C., 2005. 1881 and 1949 earthquakes atthe Chios-Cesme Strait (Aegean Sea) and their relation to tsunamis, *Nat. Hazards Earth Syst. Sci.,* **5,** 717–725.

Angelier, J., 1978. Tectonic evolution of the Hellenic Arc since the late Miocene, *Tectonophysics,* **49,** 23–36.

Angelier, J., Dumont, J.F., Karamanderesi, H., Poisson, A., Simsek, S. & Uysal, S., 1981. Analyses of fault mechanisms and expansion of southwestern Anatolia since the late Miocene, *Tectonophysics,* **75,** T1–T9.

Armijio, R., Meyer, Navarro, King, S.G. & Barka, A., 2002. Asymmetric slip partitioning in the Sea of Marmara pull-apart: a clue to propagation process of the North Anatolian Fault?, *Terra Nova,* **14,** 80–86.

Benetatos, C., Kiratzi, A., Ganas, A., Ziazia, M., Plessa, A. & Drakatos, G., 2006, Strike-slip motions in the Gulf of Siğaçik (western Turkey): properties of the 17 October 2005 earthquake seismic sequence, *Tectonophysics,* **426,** 263–279.

Bozkurt, E., 2001. Neotectonics of Turkey, a Synthesis, *Geodinamica Acta,* **14,** 3–30.

Bouchon, M., 1981. A simple method to calculate Green's functions in elastic layered media, *Bull. seism. Soc. Am*., **71,** 959–971.

Bouchon, M., 1982. The rupture mechanism of the Coyote Lake earthquake of 6 August 1979 inferred from near-field data, *Bull. seism. Soc. Am*., **72,** 745–757.

Bouchon, M., Toksöz, M.N., Karabulut, H., Bouin, M.P., Dietrich, M., Aktar, M. & Edie, M., 2000. Seismic imaging of the Izmit rupture inferred from the near-fault recordings, *Geophys. Res. Lett*., **27,** 3013–3016.

Dewey, J.F. & Sengör, A.M.C., 1979. Aegean and surrounding regions: complex multiple and continuum tectonics in a convergent zone, *Geol. Soc. Am. Bull*., **90,** 84–92.

Eyidoğan, H. & Jackson, J.A., 1985. A seismological study of normal faulting in the Demirci, Alasehir, and Gediz earthquakes of 1969-1970 in the western Turkey: implications for the nature geometry and deformation in the continental crust, *Geophys. J. R. Astr. Soc*., **81,** 569–607.

Emre, O. & Barka, A., 2000. Active faults between Gediz graben and Aegean Sea (Izmir region). *BAD SEM 2000 Symp., Izmir. Abstract*.

Emre, O., Dogan, A., Ozalp, S. & Yildirim, C., 2005. The 17 October Sıgacık earthquake preliminary report, Mineral Research Institute, No. 10756, Ankara (in Turkish).

Ganas, A., Drakatos, G., Pavlides, S., Stavrakakis, G., Ziazia, M., Sokos, E. & Karastathis, V., 2005. The 2001 Mw = 6.4 Skyros earthquake, conjugate strike slip faulting and spatial variation in stress within the central Aegean Sea, *J. Geodyn.,* **39,** 61–77.

Gautier, P., Brun, J.P., Moriceau, R., Sokoulis, D., Martinod, J. & Jolivet, L., 1999. Timing, kinematics and cause of Aegean extension, a senario based on a comparison with simple analogue experiments, *Tectonophysics,* **315,** 31–72.

Genç, C., Altunkaynak, S., Karacık, Z., Yazman, M. & Yılmaz, Y., 2001. The Cubukludag graben, south of Izmir: tectonic significance in the Neogene geological evolution of the Western Anatolia, *Geodin. Acta,* **14,** 1–12.

Goldsworthy, M., Jackson, J. & Haines, J., 2002. The continuity of active fault systems in Greece, *Geophys. J. Int*., **148,** 596–618.

Hurst, K. *et al*., 2000. Global Positioning System constraints on plate kinematics and dynamics in the eastern Mediterranean and Caucasus, *J. geophys. Res*., **105,** 5695–5720.

Hudnut, K.W., Seeber, L. & Pacheco, J., 1989. Cross-fault triggering in the November 1987 Superstition Hills earthquakes sequence, Southern California, *Geoph. Res. Letters*., **16,** 199–202.

Kahle, H.G. *et al*., 1998. The strain rate field in the eastern Mediterranean region, estimated by repeated GPS measurements, *Tectonophysics,* **294,** 237–252.

Karabulut, H., Roumelioti, R., Benetatos, C.,Mutlu, A.K., Özalaybey, S., Aktar, M. & Kiratzi, A., 2006. A source study of the 6 July 2003 (Mw 5.7) earthquake sequence in the Gulf of Saros (Northern Aegean Sea): new evidence for the western continuation of the Ganos fault, *Tectonophysics,* **412,** 195–216.

Kelly, P.G., Sanderson, D.J. & Peacock, D.C., 1998. Linkage and evolution of conjugate strike-slip fault zones in Limestones of Somerset and Northumbria, *J. Struct. Geol.,* **20**(11), 1477–1493.

Kiratzi, A. & Louvari, E., 2003. Focal mechanisms of shallow earthquakes in the Aegean Sea and the surrounding lands determined by waveform modeling: a new database, *J. Geodyn.,* **36,** 251–274.

Kissling, E., Ellsworth, W.L., Eberhart-Phillips, D. & Kradolfer, U., 1994. Initial reference models in local earthquake tomography, *J. geophys. Res*., **99**(B10), 19635–19646, doi:10.1029/93JB03138.

Klein, F.W., 1989. User's guide to HYPOINVERSE, a program for VAX computers to solve earthquake locations and magnitudes: U.S. Geological Survey Open-File Report 89-314, 58 p.

Kurt, H., Demirbag, E. & Kuscu, I., 1999. Investigation of the submarine active tectonism in the Gulf of Gokova, southwest Anatolia–southeast Aegean Sea, by multi-channel seismic reflection data, *Tectonophysics,* **305,** 477–496.

Le Pichon, X. & Angelier, J., 1979. The Hellenic arc and trench system: a key to the neotectonic evolution of the EasternMediterranean area, *Tectonophysics,* **60,** 1–42.

Le Pichon, X. & Angelier, J., 1981. The Aegean Sea, *Philos. Trans. R. Soc. Lond.,* **A300,** 357–372.

Le Pichon, X. *et al*., 2001. The active Main Marmara Fault, *Earth Planet. Sci. Lett.,* **192,** 595–616

Lin, G. & Shearer, P., 2005. Tests of relative earthquake location techniques using synthetic data, *J. geophys. Res*., **110,** B04304, doi:10.1029/2004JB003380, 2005.

Lykousis, V.C., Anagnostou, C., Pavlakis, P., Rousakis, G. & Alexandri, M., 1995. Quaternary sedimentary history and neotectonic evalution of the eastern part of Central Aegean Sea, Greece, Marine, *Geology,* **128,**

McKenzie, D.P., 1972. Active tectonics of Mediterranean region, *Geophys. J. R. Astron. Soc*., **30,** 109–185.

McKenzie, D., 1978. Active tectonics of the Alpine-Himalayan belt: the Aegean Sea and surrounding regions, *Geophys. J. R. Astron. Soc*., **55,** 217–254.

McClusky, S. *et al.*, 2000. Global Positioning system constraints on plate kinematics and dynamics in the eastern Mediterranean and Caucasus, *J. geophys. Res*., **105,** 5695–5719.

Nyst, M. & Thatcher, T., 2004. New constraints on the active tectonic deformation of the Aegean, *J. geophys. Res*., **109,** B11406, doi:10.1029/2003JB002830, 2004.

Ocakoğlu, N., Demirbağ, E. & Kuşçu, I., 2004. Neotectonic structures in the area off shore of Alaçati, Doğanbey and Kuşadasi (westernTurkey): evidence of strike-slip faulting in the Aegean extensional province, *Tectonophysics,* **391,** 67–83.

Ocakoğlu, N., Demirbağ, E. & Kuşçu, I., 2005. Neotectonic structures in İzmir Gulf and surrounding regions (westernTurkey): evidences of strike-slip faulting with compression in the Aegean extensional regime, *Mar. Geol*., **219,** 155–171.

Özalaybey, S., Ergin, M., Aktar, M., Tapırdamaz, C., Biçmen, F. & Yörük, A., 2002. The 1999 Izmit earthquake sequence in Turkey: seismological and tectonic aspects, *Bull. seism. Soc. Am*., **92,** 376–386.

Şaroğlu, F., Emre, O. & Kuscu, I., 1992. Active fault map of Turkey, scale 1: 2,000,000,000 Mineral Research and Exploration Institute of Turkey.

Şengör, A.M.C., Satır, M. & Akkok, R., 1984. Timing of tectonic events in the Menderes Massif, western Turkey: implications for tectonic evolution and evidence for Pan-African basement in Turkey, *Tectonics,* **3,** 693–707.

Stein, R.S., King, G. & Lin, J., 1992. Change in failure stress on the southern San Andreas fault system caused by the 1992 Magnitude = 7.4 Landers earthquake, *Science,* **258,** 1328–1332.

Taymaz, T., Jackson, J. & McKenzie, D., 1991. Active tectonics of the north and central Aegean Sea, *Geophys. J. Int*., **106,** 433–490.

Thatcher, W. & Hill, D.P., 1991. Fault orientations in extensional and conjugate strike-slip environments and their implication, *Geology,* **19,** 1116–1120.

Waldhauser, F. & Ellsworth, W.L., 2000. A double-difference earthquake location algorithm: method and application to the northern Hayward Fault, CA, *Bull. seism. Soc. Am*., **90,** 1353–1368.

Yılmaz, Y., 1997. Geology of Western Anatolia, in *Active Tectonics of NW Anatolia - The Marmara Poly-project,* eds Schindler, C. & Pfister, M., VDF, ETH Zurich.

Yılmaz, Y., Genç, S.C., Gürer, F., Bozcu, M., Yılmaz, K., Karacık, Z., Altunkaynak, S. & Elmas, A., 2000. When did the western Anatolian grabens begin to develop? in *Tectonics and Magmatism in Turkey and Surrounding Area,* Vol. 173, pp. 353–384, eds Bozkurt, E., Winchester, J.A., Piper, J.D.A., *Geol. Soc. London Spec*. Publ.

Yeats, S., Sieh, K. & Allen, C.R. 1997. *The Geology of Earthquakes,* Oxford University Press, Oxford

APPENDIX A

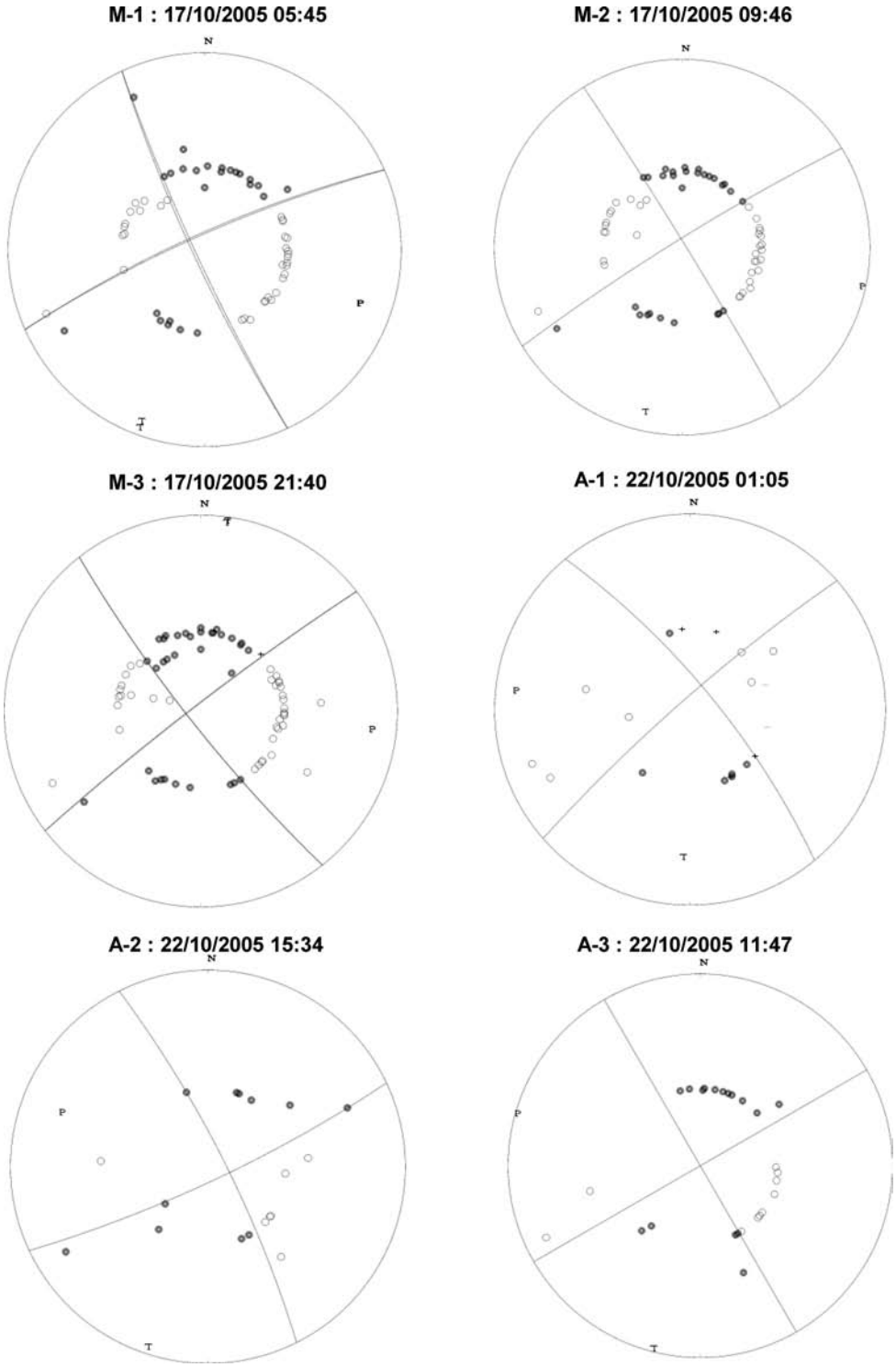

Figure A1. Focal mechanism solutions from first motion polarities of three main shocks and three aftershocks shown in Fig. 4 (a) M-1; (b) M-2; (c) M-3; (d) A-1; (e) A-2 and (f) A-3.